Supplementary Information

Programmable spherical nucleic acids integrated with MOF-confined copper nanoclusters facilitate electrochemiluminescent detection of prostate-specific biomarkers

Yi Li[a], Mei-Ling Liu[a], Wen-Jing Yang[a], Xue-Mei Zhou[b], Ying Zhuo[b*], and Xiao-Jing He[a*]

[a]*Department of Radiology, The Second Affiliated Hospital of Chongqing Medical University, Chongqing.*

[b]*Chongqing Engineering Laboratory of Nanomaterials & Sensor Technologies, College of Chemistry and Chemical Engineering, Southwest University, Chongqing.*

[*] Corresponding author at: **Tel/Fax**: +86 23 63693238; **Tel/Fax**: +86 23 68253172.

E-mail address: he_xiaojing@hospital.cqmu.edu.cn. (X. J. He); yingzhuo@swu.edu.cn. (Y. Zhuo).

Table of Contents

1. Experimental section

1.1. Reagents and materials

Copper sulfate pentahydrate ($CuSO_4 \cdot 5H_2O$), potassium persulfate ($K_2S_2O_8$), tris (2-carboxyethy) phosphine hydrochloride (TCEP) and potassium ferricyanide ($K_4[Fe(CN)_6]$) were brought from Sigma-Aldrich Co. (St. Louis, MO, USA). Zinc acetate dihydrate ($(CH_3COO)_2Zn$) was provided by the Macklin Biochemical Co., Ltd (Shanghai, China). Glutathione (GSH) and 6-mercapto-1-hexanol (MCH) were purchased from J&K Technology Co., Ltd. (Beijing, China). Sodium hydroxide (NaOH) of analytical reagent grade was supplied by Chemical Reagent Co. (Chongqing, China). N, N-dimethylformamide (DMF) was purchased from Chengdu Kelong Chemical Industry (Chengdu, China). Terephthalic acid (H_2BDC) was obtained from Qiang Shun Chemical Co. (Shanghai, China). Amino-modified Fe_3O_4 magnetic beads (NH_2-Fe_3O_4, 100-200 nm) were provided by Bejing Bailingwei Chemical Industry (Beijing, China). Ultrapure water was purified by a Millipore Milli-Q water purification system with an electric resistance of 18.2 MΩ/cm and used throughout the experiment. All reagents and solvents were used as received without further purification.

The alpha-methylacyl-CoA racemase (AMACR) was purchased from Shanghai Chemtron Biotech Co., Ltd (Shanghai, China). The common cancer biomarkers, including PTK-7, MUC1, CD63, and TB were obtained from Beijing Bioss Co., Ltd (Beijing, China). The Engen® Lba Cas12a (cpf1) and NEB buffer 2.1 were purchased

from Shanghai Titan Scientific Co., Ltd (Shanghai, China). The human AMACR enzyme-linked immunosorbent assay kit was obtained from Jiangsu enzyme immunity experiment Co., Ltd (Jiangsu, China). The Rnase-free water was purchased from Genview (Shanghai, China) to dissolve and store AMACR. HPLC-purified DNA and crRNA were obtained from Shanghai Sangon Biological Engineering Technology & Services Co., Ltd. (Shanghai, China). All the serums used in this work were acquired from the Chongqing Ninth People's Hospital. This study has been approved by the Ethics Committee and Institutional Review Boards of the hospital. The sequence information for the nucleic acids used in this study is shown in Table S1:

Table S1. Sequence information for the nucleic acids used in this study.

Name	Sequences (5' – 3')
Hairpin 1 (H1)	SH-TTT TAC ACA CCC TAC GG/idsp/ GCT AAC GGC AGA GAT TCC CCA GGT AAA CAC ACA AAC GAC TAG GGT GTG T
Hairpin 2 (H2)	SH-TTT ATG TCA TGG CCA CC/idsp/ TGC TAC AAG AGA GAA AGC CCA GGT AAA CAC ACA AAC GAC GGC CAT GAC A
Padlock	TAG CCC ACT AAG GTT TGT GTG TTT ACC TGG GCT TAA TCA ACG
Locker	ACC TTA GTG GGC TAC GTT GAT TAA GCC CAG G
Aptamer[1]	CCC TAC GGC GCT AAC CCA TGC TAC GAA TTC GTT GTT AAA CAA TAG GCC ACC GTG CTA CAA
DNA walker	TTG TAG CAC GGT GGC CAT AAC AAA TTG TTG CTT AAG CAC GGA GCG ACC TAA CCG TGC CGT TAG CGC CGT AGG G
Ferrocene-labeled DNA (Fc-DNA)	SH-$(CH_2)_6$-AAC CGC TTC CCC GAC TTC C-Fc
crRNA	UAA UUU CUA CUA AGU GUA GAU AAG GUU UGU GUG UUU ACC UG

Furthermore, the buffers applied in this study are listed as follows:

(1) 1×TE buffer (10.0 mM Tris-HCl, 1.0 mM EDTA, pH 8.0) was used to dissolve and store DNA in this study.

(2) DNA hybridization buffer (10.0 mM Tris-HCl, 1.0 mM EDTA, and 1.0 M NaCl, pH 7.0) was used as the reaction buffer for DNA hybridization.

(3) Tris-HCl (140.0 mM NaCl, 5.0 mM $CaCl_2$, 1.0 mM $MgCl_2$, pH 7.6) was used to dissolve and store Fc-DNA.

(4) The phosphate buffer saline (PBS, 0.1 M, pH 7.4) consisted of 0.1 M KH_2PO_4, 0.1 M Na_2HPO_4, and 0.1 M KCl. The $S_2O_8^{2-}$ solution (10.0 mM, pH 7.4) was prepared by dissolving the solid $K_2S_2O_8$ in 0.1 M PBS.

(5) 5×TBE buffer (445.0 mM tris, 445.0 mM boric acid, 10.0 mM EDTA, pH 8.0) was used in polyacrylamide gel electrophoresis (PAGE).

1.2. Apparatus

The electrochemical and ECL measurements were recorded on MPI-E multifunctional electrochemical and chemiluminescent analytical systems (Xi'an Remax Electronic Science &Technology Co. Ltd., Xi'an, China). Cyclic voltammetric (CV) measurements were recorded by CHI 660A electrochemistry work station (Shanghai Chenhua Instruments, China), which utilized a conventional three-electrode system including a modified glassy carbon electrode (GCE) as the working electrode, a saturated calomel electrode (SCE) as the reference electrode, and a platinum wire as the auxiliary electrode. The morphology and size of the synthesized nanomaterials were characterized by the ZEISS Gemini 300 scanning electron microscopy (SEM,

Zeiss, Germany) and FEI Tecnai G2 F20 transmission electron microscopy (TEM, FEI, USA). X-ray photoemission spectroscopy (XPS) measurement was investigated by Thermo Scientific K-Alpha (Thermo Fisher Scientific, USA). Fluorescence characterization was performed on a FL-5700 spectrophotometer (Hitachi, Tokyo, Japan). ECL spectra were analyzed by the ECL spectrum system, concluding the electrochemical workstation (Vertex, Ivium Technologies Co., Ltd., Netherlands), the spectrometer (Kymera 193i, Andor, U.S.A), and the Multi-spectral EMCCD (Newton, Andor, U.S.A) integrated with a Newton EMCCD spectroscopy detector (Andor Co., Tokyo, Japan). Native PAGE was carried out with a BG-verMIDI standard vertical electrophoresis apparatus (Baygene, China) and a Gel Doc XR+ System (Bio-Rad, USA).

1.3. The assembly process of the DNA nanostructures

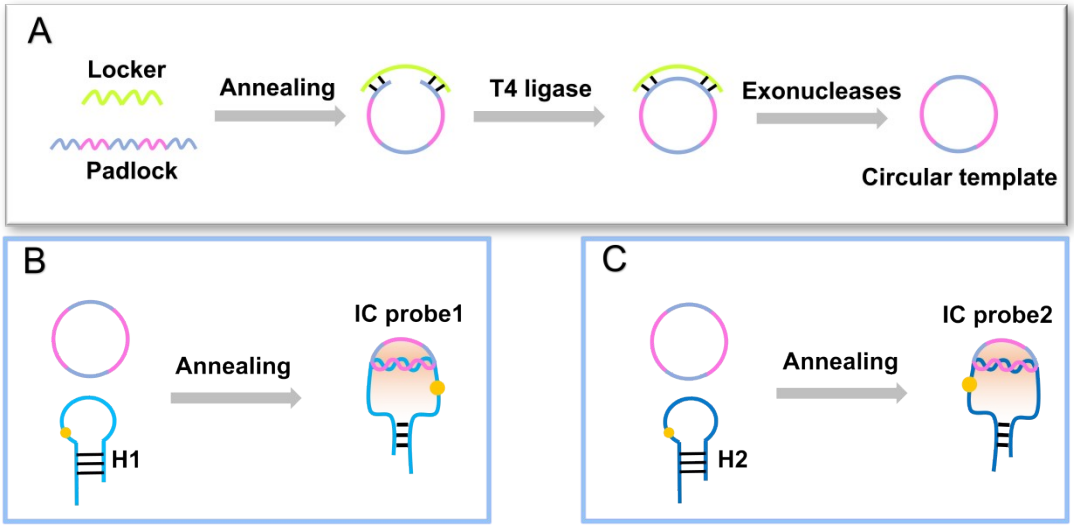

Fig. S1 The assembly process of (A) circular template, (B) IC probe1, and (C) IC probe2.

1.4. Synthesis of gold-magnetic nanoparticles (Au@Fe_3O_4)

To start with, we synthesized the Au nanoparticles (Au NPs, 16 nm) based on the classic method.[2] Specifically, 40 mL of $HAuCl_4$ (0.01%) solution was heated to boil under constant stirring. Following that, 1 mL of trisodium citrate (1%) solution was mixed with the above solution under stirring and kept boiling for 15 min. After that, the color of the solution turned wine red, demonstrating the successful synthesis of the Au NPs. Then, the mixture was cooled to room temperature and stored at 4 °C for further use.

According to the previous literature, the $Au@Fe_3O_4$ was synthesized in the following steps.[3] Briefly, 500 μL of the NH_2-Fe_3O_4 suspension was washed three times with deionized water. Then, the as-prepared Au NPs solution (3 mL) was added to the NH_2-Fe_3O_4 suspension and stirred at 4 °C for 12 h. Subsequently, the $Au@Fe_3O_4$ were obtained after magnetic separation and redispersed in PBS buffer (1 mL) for the following experiments.

2. Results and discussion

2.1. The size distribution of Cu NCs

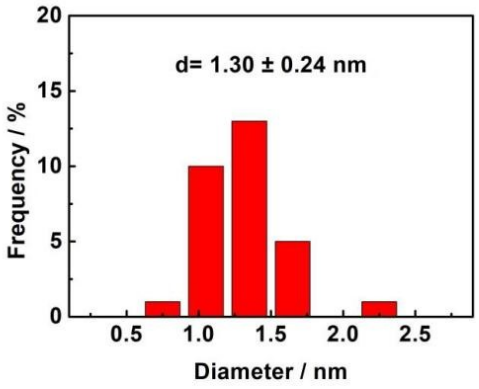

Fig. S2 The histogram of the size distribution of Cu NCs.

2.2. Inductively coupled plasma mass spectrometry (ICP-MS) analysis of Cu element in Cu NCs@Zn-MOF

Table S2. ICP-MS analysis of Cu element in Cu NCs@Zn-MOF.

Sample quality (g)	Volume (mL)	Concentration of Cu element (ug/L)	Quality of Cu element (ug/kg)	Wt (%)
0.0446	25	142441.475	78696703.222	7.86

2.3. The X-ray diffraction (XRD) and inductively coupled plasma mass spectrometry (FTIR) analysis of Cu NCs@Zn-MOF and Zn-MOF

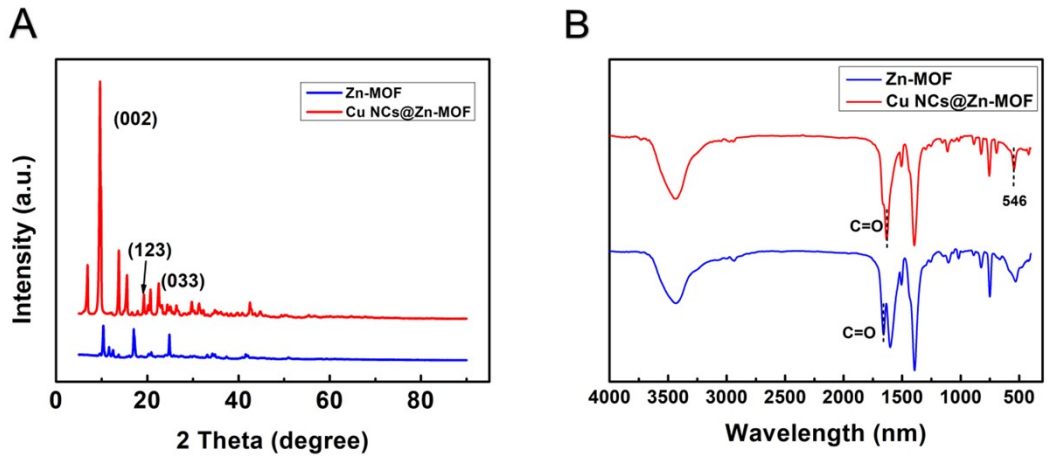

Fig. S3 The (A) XRD and (B) FTIR analysis of Cu NCs@Zn-MOF and Zn-MOF.

2.4. The TEM characterization of Au@Fe_3O_4

The morphological and size of the prepared Au@Fe_3O_4 was performed by the transmission electron microscopy (TEM) measurements. As shown in Fig. S4, the synthesized Au@Fe_3O_4 appeared as a spherical structure with an average particle size of 100 nm.

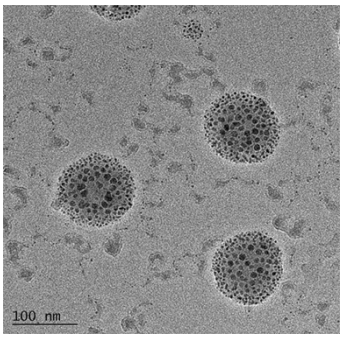

Fig. S4 The TEM characterization of Au@Fe_3O_4.

2.5. The element analysis of Cu NCs@Zn-MOF

Table S3. The element analysis of Cu NCs@Zn-MOF.

Element	C	O	Cu	Zn
Weight percentage	54.7	29	2.63	13.81

2.6. The ECL stability of Cu NCs@Zn-MOF

The ECL stability of Cu NCs@Zn-MOF was evaluated by continuously scanning at different periods. As displayed in Fig. S5A, the newly prepared Cu NCs@Zn-MOF showed excellent stability with a relative standard deviation (RSD) of 0.3%. Furthermore, after storing for a month at 4 ℃, Cu NCs@Zn-MOF exhibited the ECL response of 13435 a.u. with the RSD of 1.0% under continuous potential scanning (Fig. S5B), suggesting the satisfactory stability of Cu NCs@Zn-MOF.

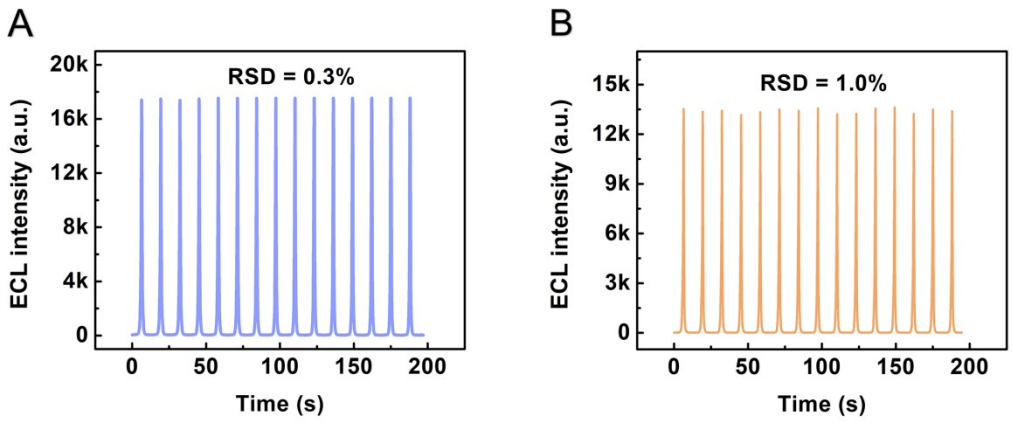

Fig. S5 The ECL stability of (A) the newly prepared Cu NCs@Zn-MOF and (B) the Cu NCs@Zn-MOF after storing for a month at 4 ℃.

2.7. The probable ECL mechanism of Cu NCs@Zn-MOF-$S_2O_8^{2-}$ system

Briefly, the Cu NCs were protonated into the radical anion of Cu NCs (Cu NCs$^{\bullet-}$). At the same time, the Zn-MOF with micro-nano structure boosted the reduction of $S_2O_8^{2-}$ to generate the strong oxidizing intermediate radical ($SO_4^{\bullet-}$). The $SO_4^{\bullet-}$ further reacted with Cu NCs$^{\bullet-}$ to form a large number of excited-state species (Cu NCs*), which returned to the ground state accompanied by the ECL emission producing. The possible emitting mechanism was depicted as the following equations:

$$\text{Cu NCs} + e^- \longrightarrow \text{Cu NCs}^{\bullet-}$$

$$S_2O_8^{2-} + e^- \xrightarrow{\text{Zn-MOF}} S_2O_8^{2-} + SO_4^{\bullet-}$$

$$SO_4^{\bullet-} + \text{Cu NCs}^{\bullet-} \longrightarrow SO_4^{2-} + \text{Cu NCs}^*$$

$$\text{Cu NCs}^* \longrightarrow \text{Cu NCs} + h\nu$$

2.8. The characterizations of biosensor establishment process

To affirm the successful assembly steps of the proposed biosensor, CV and electrochemical impedance spectroscopy (EIS) measurements were implemented

under a potential scan cycle of -2.0 ~ 0 V in 0.1 M PBS with 5 mM $[Fe(CN)_6]^{3-/4-}$. In Fig. S6A, a pair of redox peaks could be seen (curve *a*), which was attributed to the reversible redox reaction of $[Fe(CN)_6]^{3-/4-}$ on the bare GCE. When Cu NCs@Zn-MOF was dropped to the surface of the GCE, the insulated organic ligand of the Zn-MOF resulted in a reduced current (curve *b*). When incubated with Au NPs, the current of Au NPs/Cu NCs@Zn-MOF/GCE had a slight increase (curve *c*), which corresponded to the good electrical conductivity of Au NPs. Subsequently, a remarkably decreased current (curve *d*) could be observed along with the incubation of Fc-DNA due to its electrostatic repulsion. Furthermore, when MCH was modified onto the resultant electrode surface, the peak current did not change significantly (curve *e*). Finally, after incubation with the activated CRISPR/Cas12a, the redox peak current prominently increased (curve *f*), which originated from the cleavage of the Fc-DNA by the activated CRISPR/Cas12a.

EIS measurement was another approach to confirm the stepwise fabrication of the proposed biosensor, which reflected the electron transfer resistance (R_{et}) through the semicircle diameter of EIS and revealed the electron transfer kinetics of the electrode interface. As shown in Fig. S6B, a small semicircle (curve *a*) suggested a clear GCE was obtained for the construction of the biosensor. Following that, the value of R_{et} of Cu NCs@Zn-MOF/GCE (curve *b*) was increased obviously due to the insulating property of Zn-MOF. When Au NPs were dropped on the modified GCE, the R_{et} decreased (curve *c*), which might be speculated that Au NPs enlarged the effective contact area to accelerate electron transfer. A remarkably enhanced value of

R_{et} could be observed when Fc-DNA was incubated with the resultant GCE (curve *d*), which was attributed to the electronic repulsion between negatively charged Fc-DNA and $[Fe(CN)6]^{3-/4-}$. Subsequently, the MCH was decorated on the above electrode to block the unreacted sites, resulting in the further increased value of R_{et} (curve *e*). Finally, the R_{et} was decreased after the incubation with the activated CRISPR system (curve *f*), implying that the activated CRISPR system with trans-cleavage ability could release the Fc-DNA away from the electrode surface.

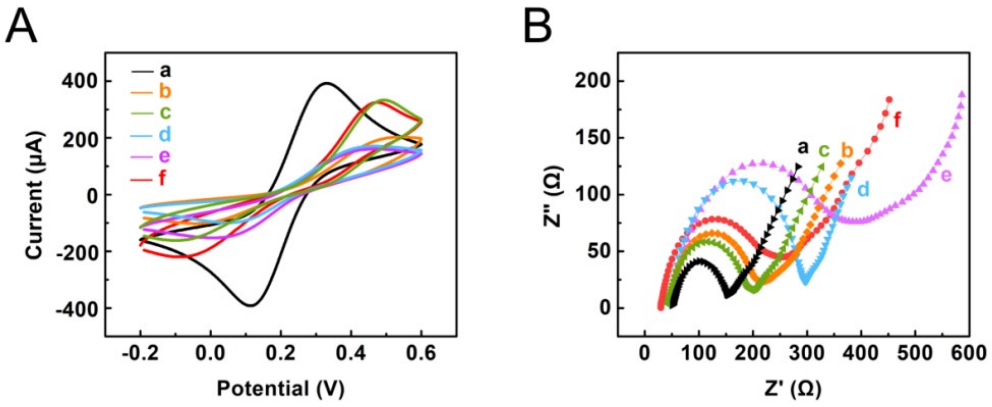

Fig. S6 CV curves (A) and EIS plots (B) of (a) bare GCE, (b) Cu NCs@Zn-MOF/GCE, (c) Au NPs/Cu NCs@Zn-MOF/GCE, (d) Fc-DNA/Au NPs/Cu NCs@Zn-MOF/GCE, (e) MCH/Fc-DNA/Au NPs/Cu NCs@Zn-MOF/GCE, and (f) the activated CRISPR system incubated with MCH/Fc-DNA/Au NPs/Cu NCs@Zn-MOF/GCE.

2.9. Quantitative analysis of band intensities in PAGE analysis

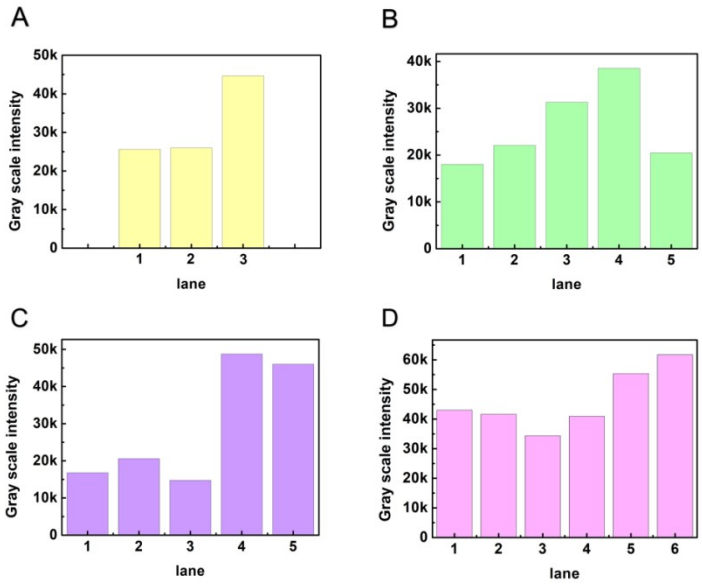

Fig. S7 Grayscale intensity of the separated bands. (A) Hybridization of DNA walker and aptamer. Lane 1, aptamer; Lane 2, DNA walker; Lane 3, hybrid products of aptamer and DNA walker. (B) Formation process of the circular templates. Lane 1, locker; Lane 2, padlock; Lane 3, locker + padlock; Lane 4, locker + padlock + T4 ligase; Lane 5, locker + padlock + T4 ligase + exonuclease I and exonuclease III. (C) Construction of the IC probes. Lane 1, circular templates; Lane 2, H1; Lane 3, H2; Lane 4, IC probe1; Lane 5, IC probe2. (D) Process of RCA reaction. Lane 1, IC probe1; Lane 2, IC probe2; Lane 3, DNA walker; Lane 4, IC probes + DNA walker; Lane 5, IC probes + DNA walker + APE1; Lane 6, IC probes + DNA walker + APE1 + phi29 DNA polymerase.

2.10. Exploration of the optimal experimental conditions

To improve the ECL detecting performances of this proposed strategy, some extremely momentous parameters about the activation time of CRISPR/Cas12a, the reaction time of RCA, and the concentration of Fc-DNA were investigated to obtain the optimal conditions. According to Fig. S8A, the ECL intensity gradually enhanced with the increase of activated time of CRISPR/Cas12a and approached a saturation point after 60 min, thus, the activated time of 60 min was chosen as the optimal time

throughout the experiment. Additionally, the RCA reaction time was an important element in improving the analytical performance of the developed sensing platform. As illustrated in Fig. S8B, it could be clearly observed that the ECL intensity consecutively increased accompanied by the increment of RCA reaction time, and reached the plateau at 60 min. Consequently, the reaction time of RCA was determined to be 60 min for the following experiments. Furthermore, the concentration of Fc-DNA was optimized as displayed in Fig. S8C. Briefly, the ECL response decreased rapidly as the concentration of Fc-DNA increased. When the concentration was at 2.0 μM, an extremely low background signal was achieved so that 2.0 μM was selected as the optimal condition to apply in the whole experiments.

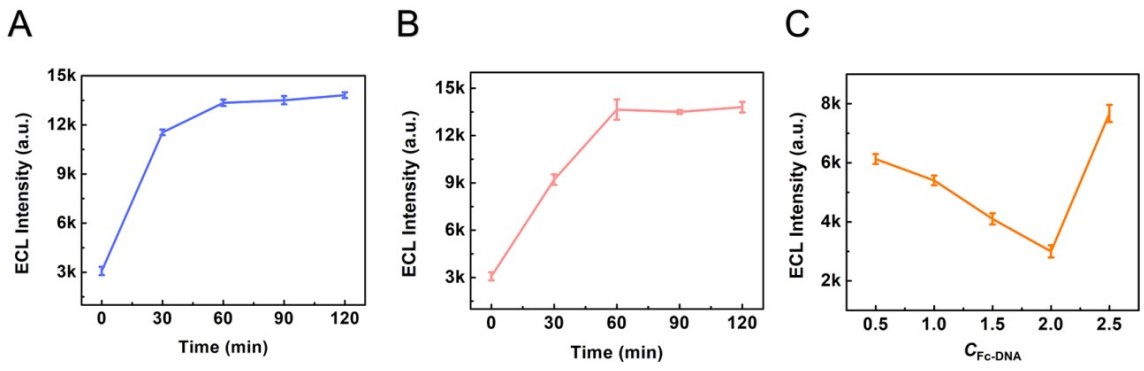

Fig. S8 Exploration for the optimal experimental conditions. Optimizations of (A) the activated time of CRISPR/Cas12a system: 0 min, 30 min, 60 min, 90 min, and 120 min, (B) the reaction time of RCA: 0 min, 30 min,60 min, 90 min, and 120 min, and (C) different concentrations of Fc-DNA: 0.5 μM, 1.0 μM, 1.5 μM, 2.0 μM, and 2.5 μM.

2.11. The calculation procedure of detection limit

According to the previously reported reference, we adopted the traditional and

typical approach to calculate the detection limit of the proposed biosensor.[4] Briefly, three parallel experiments of the blank samples were carried out, and then the average ECL intensity (I_B) was calculated to be 2323.9 a.u. with a standard deviation (S_B) of 219. When the signal-to-noise ratio value (k1) was 3, the smallest detectable ECL signal could be calculated as

$$I_L = I_B + k_1 S_B = 2980.9$$

On the basis of the linear regression equation (I = 1981.46 lg c + 7731.0), the detection limit could be calculated as 4 pg mL^{-1}.

2.12. Comparison of different methods for AMACR detection

Table S4. Comparison of different methods for AMACR detection.

Test method	Linear range	LOD	Ref
DPV	1 μg mL^{-1} ~ 10 μg mL^{-1}	50 ng mL^{-1}	5
EIA	10 pg mL^{-1} ~ 5 ng mL^{-1}	4.6 pg mL^{-1}	1
ECL	10 ng mL^{-1} ~ 100 μg mL^{-1}	1.25 ng mL^{-1}	6
ECL	1 ng mL^{-1} ~ 100 μg mL^{-1}	0.1 ng mL^{-1}	7
ECL	10 pg mL^{-1} ~ 1 μg mL^{-1}	4 pg mL^{-1}	this work

References:

[1] D. K. Yang, L. C. Chen, M. Y. Lee, C. H. Hsu and C. S. Chen, *Biosens. Bioelectron.*, 2014, **62**, 106-112.

[2] Y. Li, F. Yang, R. Yuan, X. Zhong and Y. Zhuo, *Food Chem*., 2022, **389**, 133049.

[3] T. T. Tu, Y. M. Lei, Y. Q. Chai, Y. Zhuo and R. Yuan, *ACS Appl. Mater. Interfaces.*, 2020, **12**, 3945-3952.

[4] V. A. Zamolo, G. Valenti, E. Venturelli, O. Chaloin, M. Marcaccio, S. Boscolo, V. Castagnola, S. Sosa, F. Berti, G. Fontanive, M. Poli, A. Tubaro, A. Bianco, F. Paolucci and M. Prato, *ACS Nano*, 2012, **6**, 7989-7997.

[5] J. W. Yao, Y. Wang, Y. F. Dai, C. C. Liu, *ACS Omega*. 2018, **3**, 6411-6418.

[6] M. L. Liu, Y. Li, M. L. Zhao, Y. Zhuo and X. J. He, *Biosens. Bioelectron*., 2022, **214**,114512.

[7] Y. Li, M. L. Liu, W. B. Liang, Y. Zhuo and X. J. He, *Biosens. Bioelectron*., 2023, **238**, 115589.